Dynamics of Fines Deposition in an Alternating Semifluidized Bed

S. Dehkissia, A. Baçaoui, I. Iliuta, and F. Larachi
Dept. of Chemical Engineering, Laval University, Québec, Canada G1K 7P4

DOI 10.1002/aic.11538
Published online June 4, 2008 in Wiley InterScience (www.interscience.wiley.com).

A semifluidized bed was proposed to allay bed plugging during the filtration of fines-hydrocarbon suspensions. Mitigation of plugging was allowed by alternating semifluidization during capture with unconstrained fluidization for removal of deposits. Solids holdup conditions were established to prevent deposition in the fluidization section. The cyclic parameters were varied to allow efficient removal of deposits during washing. Analysis with a filtration model accounting for solids detachment in the fixed bed section revealed that the fluidization section favored growth of aggregate size entering the fixed bed. Analysis of the split ratios between fixed and fluidized bed heights revealed that the shallowest fluidization sections delayed deposition in the fixed bed. In cyclic operation, reversibility of the semifluidized bed was best recovered via gas injection during the washing stages. However, the filtration times in successive cycles shortened with increasing washing times but lengthened with increasing the washing superficial suspension velocity. © 2008 American Institute of Chemical Engineers *AIChE J,* 54: 2120–2131, 2008

Keywords: filtration, semifluidization, cyclic operation, plugging with fines, depth filtration modeling, hydrodynamics

Introduction

Bituminous sands are promising medium-term alternatives to counter the declining supplies in conventional light crude oils.[1] Only in Canada, bitumen resources have been estimated to be 2.5–6 trillion barrels,[2] which largely exceed worldly conventional petroleum proven reserves.[3] Because of the prevailing geothermal gradient, bituminous sands are nonmobile at reservoir conditions which require adapted extraction/separation and especially upgrading methods.[4] Beside bitumen and sand, bituminous sands are complex multiphase systems which also contain fines, colloids, clay organics, nonpetroleum-derived organics, etc. Fines are defined as solid materials passing a 325-mesh sieve (<44 μm) and are comprised mostly of silt, very fine quartz, and clay minerals.[2] Before being used as a feedstock for conventional refining, the extracted/separated bitumen is upgraded to yield the so-called bitumen-derived crude. Primary upgrading by thermal cracking via C-rejection (delayed/fluid coking) or by hydrocracking via H-addition (LC-Fining)[5] produces a sulfur-rich syncrude. Secondary upgrading is required to comply with the low-sulfur specifications for the fractions to hydrotreat, especially the heavy gas oil fraction.[6] Although hydrodesulfurization at the commercial scale is carried out in a series of trickle-bed reactors, a tiny fraction of these naturally occurring fines intrude in the heavy gas oil fraction. These fines often worm into the mineral processing units upstream or escape from the cokers. Some of these solids carry over to the trickle beds because, being so fine, they are not completely stoppable by the upstream filters.[7] Although the fines/hydrocarbon suspensions fed to the trickle-bed reactors are very dilute, the cumulative effect of tens of thousands of barrels of feedstock processed each day diverts the first catalyst beds into gigantic filters collecting significant amounts of fines. Fines accumulation causes the

Correspondence concerning this article should be addressed to F. Larachi at faical.larachi@gch.ulaval.ca.
Current address of A. Baçaoui: Department of Chemistry, FSSM, Cadi-Ayyad University, Marrakesh, Morocco.

pressure to rise by restricting the flow paths of the fluids. Eventually, the bed pressure drop becomes so high that the hydrotreaters must be shutdown before the stress tolerance of the catalyst bed support is reached.[7] This leads to more frequent replacements of catalyst regardless of the chemical activity left in it. Hence, fines deposition in trickle beds was reported to prematurely shorten reactor cycle life, increase operational problems, and maintenance work and lead to poor energy efficiency. Furthermore, compliance with the ultra-low sulfur specifications prompted by tighter regulations requires the use of highly efficient sweetening catalysts which are capital-intensive. However, these catalysts are incompatible with the very high rate of catalyst replacement in trickle-bed reactors in comparison with hydrotreating catalysts used in conventional refining operations.

Recently, a few investigations referring to the study of plugging in trickle beds have become available in the literature.[8–10] These studies focused more on providing an understanding of trickle bed behavior rather than on proposing new configurations to minimize reactor shutdowns due to deposition. Deposition must be minimized so that the reactor would be *indifferent* to filtration over extended periods of time: *ideally by enabling the flow paths in the vessel to keep unhindered as in a clean state [Case 1], *or by allowing cyclic operation removing periodically the deposits being accumulated while preventing reactor disruption [Case 2]. To approach [Case 1], one option was the use of monolith reactors as an alternative to trickle beds. Because of the monolith's straight channels, the increase of pressure drop and bed specific deposit (i.e., mass of deposited fines per unit reactor volume) as filtration evolves was found to be less than in trickle beds at equal specific surface area.[11] However, the reduction in specific deposits was not spectacular suggesting that replacement of trickle beds with monoliths remains to be demonstrated. The quest for alternatives to extend operational life of hydrotreating reactors must be pursued in terms of reduction in specific deposit and pressure buildup.

Some of the earlier semifluidized bed applications concerned biological reactions. These reactors consist of an assemblage of a fluidized section topped by a packed bed within a single vessel.[12,13] Inception of semifluidization occurs when a mass of fluidized particles is compressed by the fluidizing fluid against a restraining top grid to limit bed expansion.[14–16] In semifluidized beds, the fluidized layer exhibits the highest backmixing and carries the main load of biological reaction, whereas the top packed bed acts as a polishing section.[13] When the packed bed section is plugged by cell mass or suspended solids, it is cleared by raising periodically the guard grid. This helps removing the trapped materials by hydrodynamic shear stress. Wen and Fan[17] described a smart semifluidization setup in which capture of fines can be maximized, not by promoting their trapping in the fixed bed section, but rather by retaining them in the lowermost fluidized section. Accumulation of the deposits is ensured by progressively or intermittently lifting the grid. Refluidizing proportionally the fixed-bed bottom part helps breaking the cake being formed in the previously immobile collecting particles. During the filtration cycle, as the fixed bed is thinning in proportion as the fluidized section is enlarging, the filtered solids build up almost exclusively in the fluidized portion. This arrangement implies discontinuous operation as a fluid is required in subsequent fluidization cleaning cycle to purge the filtered particles via the disengaging freeboard.

The concept of filtration in semifluidized beds as advocated in the applications of Fan and coworkers[17,18] was nevertheless devised to maximize capture of fines from suspension flows. This would achieve exactly the *opposite* of what is desired for our problem. In addition, considering the high severity of hydrotreating reactions, it may be unrealistic to transpose grid translation in an industrial-scale unit. The same cyclic operation could be approached [Case 2] by alternating a semifluidized state at higher semifluidization velocity (U_{Lsf}) with occasionally a state of unconstrained fluidization at lower liquid velocity (U_L). This is illustrated in Figure 1 as alternating semifluidization. The fixed bed top layer is cleared with ease depending on the threshold pressure drop not to be exceeded during plugging. Semifluidization requires $U_{Lsf} > U_{Lmf}$ (i.e., the minimum fluidization velocity). By judiciously setting the ratio between the fixed/fluidized bed heights, there would be an operating window $U_{Lmf} < U_L < U_{Lsf}$ for attaining full refluidization. This would remove the fines that have been trapped by forcing the *entire* top fixed bed layer to periodically collapse. Moreover, because of permanent particle–particle and particle–wall collisions, deposition can be prevented in the bottom fluidized bed layer. This bottom section would act as a *self-cleaning* filter especially if filtration-free conditions can be identified. In return, this layer promotes liquid and solids backmixing[13,19] which are not desirable in hydrotreating reactors where nearness to plug flow is critical. However, it is a matter of process optimization to reduce the height of the fluidized layer so that chemical performance is not compromised. Moreover, the resulting slightly lower catalyst load per unit vessel volume lowers productivity. However, this should largely be counterbalanced by a significantly improved life cycle of the process. As hydrogenation is highly exothermic, an extra-side benefit of a semifluidized bed would be an efficient smoothing out of temperature gradients inside the hydrotreater.

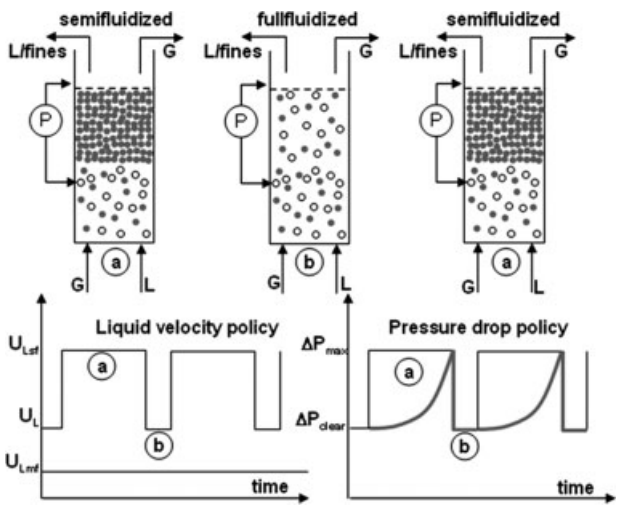

Figure 1. Concept of alternating semifluidized beds (a) semifluidized bed state at U_{Lsf}, (b) fully fluidized bed state at $U_{Lmf} \leq U_L \leq U_{Lsf}$.

See also liquid feed and pressure drop policies.

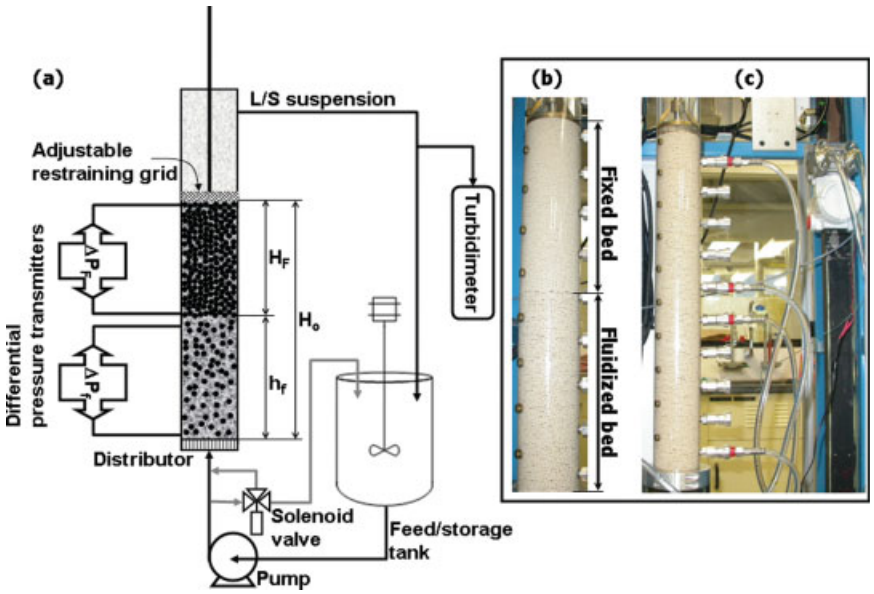

Figure 2. (a) Semifluidized bed experimental setup; (b) demarcation between fixed and fluidized bed sections; (c) bed in washing cycle fully fluidized and location of pressure taps.

[Color figure can be viewed in the online issue, which is available at www.interscience.wiley.com.]

The objective of this work was to study the feasibility of a semifluidized bed reactor as a replacement solution of fixed beds for the mitigation of plugging under various conditions of liquid superficial velocity and split ratio R. The effects during the washing cycles of wash time, gas and liquid superficial velocities, and introduction of surfactants were also examined. The rate of deposition, the suspension residual concentration, and the pressure gradients in fixed and fluidized bed sections were monitored in time using kerosene/kaolin suspensions.

Experimental Setup

The experiments were carried out at room temperature and atmospheric pressure using an acrylic column (D = 5.7 cm I.D. and 80 cm high) packed with 2.4 mm porous spherical alumina catalysts. The semifluidized bed height, H_o, was delineated by encompassing the packing between a perforated plate, acting as a distributor and placed at the column bottom, and a vertically sliding and adjustable restraining grid installed at the top, Figure 2a. The distributor perforated plate consisted of 225 holes, each 1.6 mm in diameter, and arranged in seven equidistant concentric circles. Despite an open area of ~18%, it was verified visually to give uniform inlet distribution. The mesh opening of the restraining grid had a square shape 1 × 1 mm^2 which prevented the collectors (i.e., packing elements) from crossing over. However, the passage of the exiting liquid-fines suspension remained unhindered. The restraining grid allowed the fixed bed layer to form adjacent its underside by halting the expansion of fluidization (Figure 2b). This was achieved with superficial velocities in excess of the minimum semifluidization. The minimum semifluidization velocity, U_{Lmsf}, which is larger than the minimal fluidization velocity, U_{Lmf} (Figure 1), is defined as the superficial velocity whereby a first *static* layer of packing elements forms underneath the restraining grid.[13] Twenty pressure taps, 12.5 mm apart arranged as shown in Figure 2c, allowed measuring the pressure gradient across the fluidized bed, the fixed bed as well as across the restraining grid. Measurement over the latter enabled access to the minimum semifluidization velocity.

Kaolin–kerosene dilute mixtures, 1–1.5 g/L in concentrations, were the test suspensions. Kaolin was used because it is a major component of the clay minerals in the sand deposits,[2,20] whereas kerosene (ρ_L = 785 kg/m^3, μ_L = 1.54 mPa s) was selected as a model hydrocarbon liquid.[8] The catalyst was immersed in kerosene overnight to achieve bed full wetting and imbibition of the intraparticle porous volume. The bulk density of the kerosene–imbibed alumina particles was 1319 kg/m^3. The extra-granular (fixed-bed) and intraparticle porosities were 36.2 and 74.3%, respectively. The (liquid or) suspension superficial velocities were varied within the [2.8–9.0 cm/s] range. The corresponding fixed-to-fluidized bed height split ratios, $R = H_F/h_f$, were varied from 6×10^{-3} to 5 in addition to tests for $R = 0$ (unconstrained fluidization) and $R = \infty$ (full fixed bed with grid restriction). The fitted Richardson-Zaki parameters n and terminal velocity, U_∞, were (3.1, 0.14 m/s).

The suspension was pumped from a feed/storage agitated tank and was fed to the column bottom through the perforated plate. It flowed, successively, through a fluidized-bed layer of height h_f then a fixed-bed layer of height H_F. It was recirculated via the feed/storage tank in a multipass mode. Most of the capture of fines had to take place in the fixed-bed portion H_F provided the solids holdup in the fluidized bed section was carefully chosen. The connecting pipes to pump and tank from the column were positioned as vertically as possible to avoid deposition in the lines. The concentration of fines in the suspension was measured by sampling in the feed/storage reservoir at regular time intervals using a turbidimeter (Hach model 2100N). This allowed the overall specific deposit (mass of fines per unit volume) to be esti-

mated. The initial pressure drop, ΔP_{clear}, across the clean beds was determined by circulating kaolin-free kerosene at equal superficial velocities.

A solenoid valve allowed switching between a suspension superficial velocity, U_{Lsf} ($> U_{Lmsf}$ during sequence [a], Figure 1), and a lower superficial velocity, U_L ($U_{Lsf} > U_L > U_{Lmf}$ during sequence [b], Figure 1), to clean the "plugged" fixed bed by fluidizing the whole height H_o (Figure 2c). Switching was prompted once the pressure gradient in the fixed bed section reached a prescribed maximum ΔP_{max} (Figure 1). Resumption of the semifluidized bed state took place when the turbidity in the tank reached a value close to the turbidity of the starting suspension.

The amount of deposit was expressed in terms of bed specific deposit, σ, defined as the mass of fines trapped per unit volume (empty reactor basis, V_R). For experiments in multipass recirculation of the suspension, σ was obtained through a mass balance of the feed/storage tank (V_T):

$$\sigma(t) = [C_T(t=0) - C_T(t)]\frac{V_T}{V_R} \tag{1}$$

Unless otherwise stated, V_R designates the reactor portion wherein capture takes place. For instance, if capture occurs solely in the fixed bed section, then $V_R = \pi/4D^2H_F$.

An overall measure of the bed to capture fines can be made via the bed overall capture efficiency. This assumes a linear relationship between the mass flux of fines (in the multipass recirculating suspension) and the accumulation rate of fines trapped in the bed:

$$E(\sigma) = \frac{V_R}{QC_T(t)}\frac{d\sigma}{dt} \tag{2}$$

Aided with Eq. 1, Eq. 2 yields:

$$E(\sigma) = -\frac{V_T}{Q}\frac{d\ln C_T}{dt} \tag{3}$$

Monitoring the decay in time of the tank suspension concentration yields the variation of the overall capture efficiency as a function of specific deposit.[21] Alternatively, the overall capture efficiency can be expressed as a function of bed entrance and exit suspension concentration in single-pass runs as:[22]

$$E = \frac{C_{ln} - C_{out}}{C_{ln}} \tag{4}$$

Aided with the definition of the filter coefficient averaged over the bed length L:

$$\langle\lambda\rangle L = \ln\left(\frac{C_{ln}}{C_{out}}\right) \tag{5}$$

an estimation of the bed-average filter coefficient can be obtained from knowledge of the overall capture efficiency (Eq. 3) and combination of Eqs. 4 and 5:

$$E = 1 - e^{-\langle\lambda\rangle L} \tag{6}$$

In Eqs. 5 and 6, $L = H_F$ (respectively, $L = H_o$) is the fixed bed height (respectively, the total semifluidized bed height) through which capture may be taking place.

Governing equations for filtration in fixed bed section

As depicted in Figure 1, a semifluidization state is established on imposing a fluid velocity $> U_{Lmsf}$ whereby a fixed bed forms on top of a fluidized layer. The model assumes that the semifluidization operating conditions were adjusted so as to cause deposition of fines solely in the uppermost fixed-bed section. An upflowing suspension through a porous medium of uniform initial porosity ε^o and single-sized packing particles was considered along with unidirectional, isothermal, incompressible, viscous Newtonian, unreactive assumptions. Additional assumptions of the formulation were:

- The density and viscosity of the suspension were equal to those of the liquid.
- The coupling between suspension and stationary solid was realized via the fines filter rate equation, the interfacial drag force, and detachment rates for Brownian and non-Brownian fines.
- The release of Brownian fines ($d_f < 2$ μm) from the collector surface was controlled by the colloidal forces,[23,24] whereas the detachment of non-Brownian fines ($d_f > 2$ μm) was induced hydrodynamically.[24]

The model equations consist of the continuity (Eq. 7) and Navier-Stokes (Eq. 10) equations for the suspension phase, the continuity equation for the solid stationary phase (Eq. 8) and the species balance equation for the fines (Eq. 9) which migrate from suspension to solid phase.

Continuity for suspension and solid phases

$$\frac{\partial}{\partial t}\varepsilon\rho_L + \frac{\partial}{\partial z}\varepsilon\rho_L v_{Lsf} = -\gamma\rho_f N + (1-\gamma)\rho_f r^h_{det} + \rho_f r^c_{det} \tag{7}$$

$$\frac{\partial}{\partial t}[(1-\varepsilon^\circ)\rho_s + (1-\varepsilon_d)(\varepsilon^\circ - \varepsilon)\rho_f] = \gamma\rho_f N - (1-\gamma)\rho_f r^h_{det} - \rho_f r^c_{det} \tag{8}$$

Transport equation for fines

$$\frac{\partial}{\partial t}\varepsilon C + v_{Lsf}\frac{\partial}{\partial z}\varepsilon C = -\gamma N + (1-\gamma)r^h_{det} + r^c_{det} + D_L\frac{\partial^2}{\partial z^2}\varepsilon C \tag{9}$$

Momentum balance equations for suspension phase

$$\frac{\partial}{\partial t}\rho_L\varepsilon v_{Lsf} + v_{Lsf}\frac{\partial}{\partial z}\varepsilon\rho_L v_{Lsf} = \varepsilon\mu^e_L\frac{\partial^2}{\partial z^2}v_{Lsf} - \varepsilon\frac{\partial}{\partial z}P - \varepsilon\rho_L g - F_{LS} \tag{10}$$

In the case of non-Brownian fines, the rate of colloidal particle detachment is negligible, i.e., $r^c_{det} = 0$. Similarly, in the case of Brownian particles, the rate of hydrodynamic detachment is negligible, i.e., $r^c_{det} = 0$. In the equations, P stands for pressure, ε, ρ_L, and v_{Lsf} designate, respectively, the local time-evolving bed porosity, the liquid density, and the longitudinal *interstitial* semifluidization velocity, $v_{Lsf} = U_{Lsf}/\varepsilon$. F_{LS} is the interfacial drag force per unit reactor volume exerted at the interface between the suspension and the packing. The suspension effective viscosity, μ^e_L, which arises from the combination of the viscous and pseudo-turbulence stress tensors is formulated as proposed by Dankworth et al.[25] In addition, ε_d is the porosity of fines deposit, C is the local fines concentration, N is the local filtration rate, and

γ is the fraction of collector surface area available for adhesion.[26]

Constitutive equations

In the momentum balance Eq. 10, a constitutive equation is required for the interfacial drag force. The suspension behaves as a continuous medium for which the Kozeny-Carman theory can be applied for predicting the liquid-solid drag force.[27]

An Iwasaki logarithmic law[28] was used to express the dependence between the deposition rate, the fines concentration, and the superficial liquid velocity U_{Lsf}: The expressions developed by Tien and coworkers[29,30] were used to compute the filter coefficients, respectively, for the monolayer ($\sigma \leq \sigma_{cr}$) and multi-layer ($\sigma > \sigma_{cr}$) depositions.

The net local accumulation rate of fines trapped on the collectors is an outcome between the rate of filtration and the detachment rates by both Brownian and non-Brownian mechanisms[22]:

$$\frac{d\sigma}{dt} = \gamma N - (1-\gamma) r^h_{\text{det}} - r^c_{\text{det}} \tag{11}$$

The detachment rate for colloidally induced release assumes diffusion of detached colloids across the boundary layer surrounding the collector surfaces in the absence of an energy barrier[23]:

$$r^c_{\text{det}} = \alpha^c_{\text{det}} \overline{a}(1-\varepsilon) d_f \sigma \tag{12}$$

where α^c_{det} is the 1st-order release rate coefficient reflecting diffusive transport of detached colloids across the diffusion boundary layer and is computed using a colloid diffusion coefficient and the boundary layer thickness.[23]

For non-Brownian fines, the rate of hydrodynamic detachment was taken to be proportional to the difference between the wall shear stress (τ_w) and a critical shear stress (τ_{cr})[24,31]:

$$r^h_{\text{det}} = \begin{cases} \alpha^h_{\text{det}} \rho_f^{-1} \overline{a}(1-\varepsilon)(\tau_w - \tau_{cr}) & \tau_w > \tau_{cr} \\ 0 & \tau_w < \tau_{cr} \end{cases} \tag{13}$$

Equation 13 indicates that to initiate the release of fines, a wall shear stress at least equal to a critical shear stress must be exerted at the collector surface as a result of suspension flow. In other words, the critical shear stress which is an indicator of the strength of intraparticle bonds binding the fines to the collector wall must be overcome hydrodynamically. For Brownian fines, such release by hydrodynamic forces is not possible because of the much higher values of critical shear stress required for detachment. The shear stress acting on the collector was estimated using the Happel's model.[26] The critical shear stress was estimated from the condition of equilibrium between the tangential drag force exerted by the flowing suspension which tends to detach the fines and the tangential friction force opposed to sliding of the fines to preserve the deposit integrity[26]:

$$\tau_{cr} = \frac{k_f (1-\varepsilon^\circ) Ha}{5.102 \pi d_f d_p^\circ \delta^2} \tag{14}$$

where δ is the separation distance between the fine and the collector plane, Ha is the Hamaker constant, and k_f is a sliding friction coefficient.

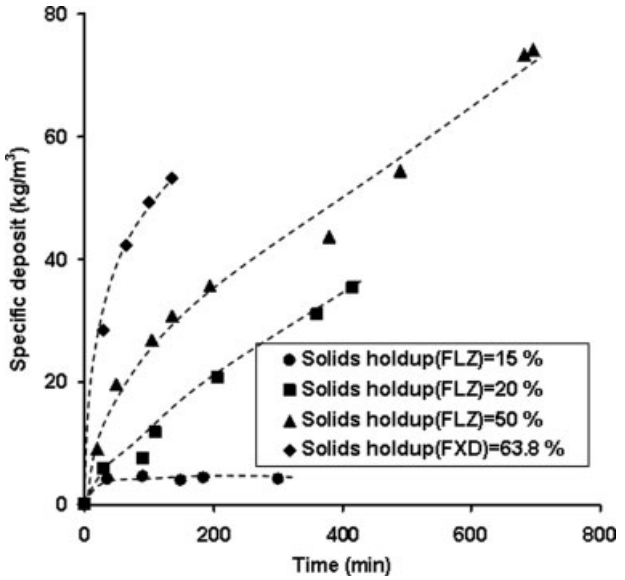

Figure 3. Time evolution of specific deposit in unconstrained fluidization (ε_{So} = 15%; h_f = 0.582 m; U_L = 0.09 m/s – ε_{So} = 20%; h_f = 0.442 m; U_L = 0.07 m/s – ε_{So} = 50%; h_f = 0.249 m; U_L = 0.03 m/s) vs. solitary fixed bed (ε_{So} = 63.8%; h_o = 0.21 m; U_L = 0.03 m/s).

Dashed lines show trends only.

Results and Discussion

Capture of fines in (unconstrained) fluidization

The capture of fines in unconstrained fluidization was analyzed to set the conditions for preventing fines deposition in the fluidized section. Runs were performed for three different initial solids holdups, ε_{So}, adjusted with varying superficial velocities: ε_{So} = 15% at U_L = 0.09 m/s, ε_{So} = 20% at U_L = 0.07 m/s, ε_{So} = 50% at U_L = 0.03 m/s, and corresponding to expanded bed heights of 0.582, 0.442, and 0.249 m, respectively. A comparative test was also included at U_L = 0.03 m/s with a fixed bed (ε_{So} = 63.8%, h_o = 0.21 m) whose height was adjusted to yield a volume of alumina spheres comparable to that of the fluidization test at U_L = 0.03 m/s.

The time evolution of the specific deposits for the four runs is illustrated in Figure 3 (dashed lines show trends and not simulated curves). The solitary fixed bed plugged, as expected, more rapidly and exhibited, at the same instants, the highest specific deposit values with respect to the fluidized configurations. Figure 3 also shows that below a threshold initial solids holdup of ca. 15–20%, deposition of fines in the fluidized bed was minor ($\sigma \approx 4$ kg/m^3). This was confirmed visually which revealed that catalyst collectors kept fairly clean. Note that this value for the specific deposit ($\sigma \approx 4$ kg/m^3) compared well with the critical specific deposit, σ_{cr}, corresponding to the number of fines required for completing a monolayer with a porosity ε_d.[32] For example, using crude estimates for $d_f \approx 10$ μm, $\varepsilon_d \approx 0.8$, and a kaolin density ρ_f = 2620 kg/m^3, yielded $\sigma_{cr} \approx 3$ kg/m^3. For larger initial solids holdup, the specific deposits increased monotonically with increasing ε_{So}. The resulting retention of fines gave its milky appearance to the fluidized layer. This milkiness was caused by the detachment of aggregates from the collectors.

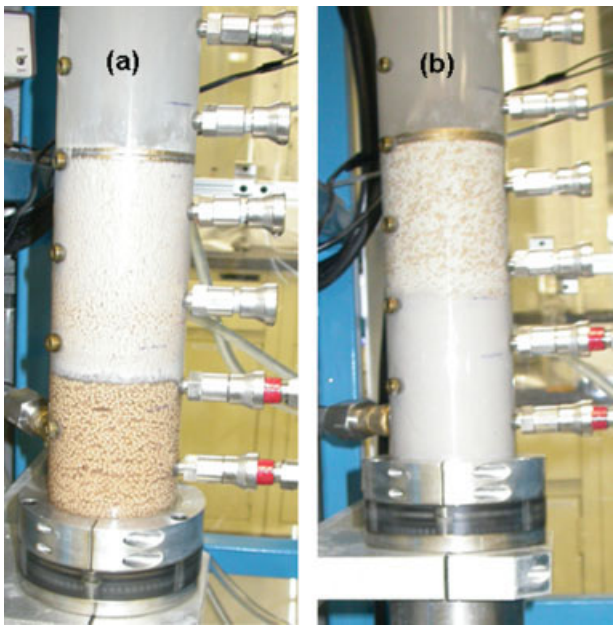

Figure 4. (a) Accumulation-free fluidized bed section in semifluidized bed U_{Lsf} = 0.054 m/s; H_o = 0.255 m, ε_{So} = 32%; (b) fines accumulation in fluidized bed section in semifluidized bed U_{Lsf} = 0.028 m/s; H_o = 0.255 m, ε_{So} = 42.6%.

[Color figure can be viewed in the online issue, which is available at www.interscience.wiley.com.]

Unlike in fixed bed depth filtration, retention of fines in fluidized beds is contributed by the aggregates trapped in the interstitial fluid.

The upper holdup limit $\varepsilon_{So} \approx$ 15–20% ensuring accumulation-free unconstrained fluidization was verified visually and was confirmed from measured specific deposits. Considering the setup as used in this work with a recirculating suspension, it was not sure that such ε_{So} limit would prevail too in semifluidization. It was anticipated—and in fact indirect evidences shall be provided later—that the aggregates being detached in the fluidized section would have sizes greater than the fines in the original suspension. This would cause the fixed bed layer located on top to plug more prematurely as compared with solitary fixed beds. Hence, recirculating suspensions coming in contact with the fluidized section in semifluidization would contain less larger-size aggregates than in unconstrained fluidization. The result would be a larger ε_{So} threshold (and, thus a lower suspension velocity, $U_L > U_{Lmf}$) for the lowermost fluidized section. This was confirmed through visual observations in Figures 4a, b. An accumulation-free fluidized section was observed at U_{Lsf} = 0.054 m/s with ε_{So} = 32% (>15%). Whereas, a milky appearance revealed substantial accumulation of fines in the fluidized section at U_{Lsf} = 0.028 m/s with ε_{So} = 42.6%. Although both fixed beds captured fines, it was considered that in semifluidization the upper limit for ε_{So} to prevent accumulation in the fluidized bed section must be ca. 32% for the alumina/ kerosene suspension.

Effect of semifluidization velocity on fines deposition

Figures 5a,b depict the evolution in time of the normalized pressure gradient, $\Delta P/\Delta P_{clean}$, and corresponding specific deposit, σ, as a function of semifluidization velocity: 0.028 m/s (H_F = 0.3 m), 0.042 m/s (H_F = 0.33 m), 0.064 m/s (H_F = 0.33 m). A split ratio R = 2 was used. Both ΔP_{clean} and ΔP were measured across the fixed bed section. The pressure loss, ΔP_{clean}, across the clean bed was measured before filtration. As discussed earlier, for U_{Lsf} = 0.042 and 0.064 m/s, only the upper fixed bed captured fines. The normalization volume V_R in Eq. 1 was $V_R = \pi/4D^2H_F$. For U_{Lsf} = 0.028 m/s capture took place both in fluidized and fixed sections so specific deposits were normalized with respect to whole semifluidized bed volume ($V_R = \pi/4D^2H_o$).

An increase in U_{Lsf} led to an increase in the time required to magnify by the same factor the normalized pressure gradient (Figure 5a) because of lesser capture by the fixed beds (Figure 5b). The dependence of $\Delta P/\Delta P_{clean}$ to liquid velocity suggests a sensitivity of deposition structure to flow conditions. With increasing liquid superficial velocity the tendency for the overall specific deposits was to decrease (Figure 5b).

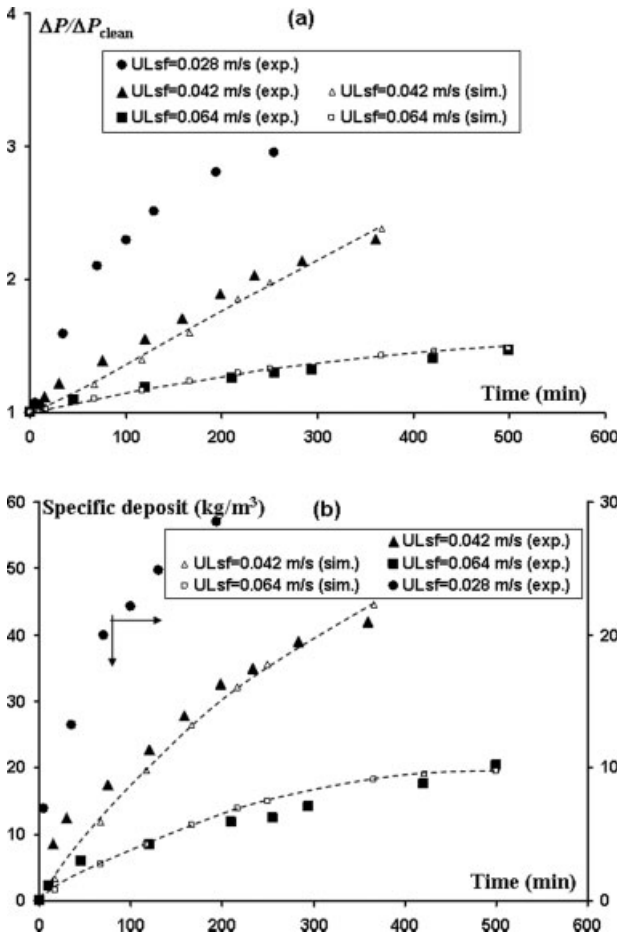

Figure 5. Effect of suspension semifluidization superficial velocity on (a) normalized pressure drop vs. time, (b) specific deposit vs. time (U_{Lsf} = 0.028 m/s; H_F = 0.3 m), (U_{Lsf} = 0.042 m/s, H_F = 0.33 m), (U_{Lsf} = 0.064 m/s, H_F = 0.33 m), R = 2.

Dotted lines/empty symbols shows simulations by depth filtration model Eqs. 7–14.

The time evolution of measured normalized pressure drop and specific deposit was compared with their simulated counterparts using the depth filtration model, Eqs. 7–14. Only the U_{Lsf} values for which deposition occurred in the fixed bed section ($\varepsilon_{So} \leq 32\%$) were considered. The run at U_{Lsf} = 0.028 m/s was excluded in the simulation because of fines trapping in the fluidized section too.

It is worthy of notice that the model is only descriptive as it requires two adjustable parameters, namely, the aggregate diameter, d_f, and the release rate coefficient α^c_{det} (colloidal first-order release rate coefficient for $d_f < 2$ μm) or α^h_{det} (hydrodynamic release rate coefficient for $d_f > 2$ μm). The aggregate diameter providing the fits illustrated in Figures 5a, b was 8 μm for both runs at U_{Lsf} = 0.042 and 0.064 m/s. This size corresponded to non-Brownian fines. The fitted hydrodynamic release rate coefficients, α^h_{det}, were 1.5×10^{-8} s/m for U_{Lsf} = 0.042 m/s and 8.5×10^{-8} s/m for U_{Lsf} = 0.064 m/s. To match the experiments for the run at U_{Lsf} = 0.064 m/s, a boost by a factor 17/3 of the hydrodynamic release rate coefficient was required with respect to that for U_{Lsf} = 0.042 m/s. As seen from Eq. 13, higher values for the hydrodynamic release rate coefficient translate into higher values for the rate of hydrodynamic particle entrainment. Hence, provided the prevailing hydrodynamic shear stress exceeds the critical shear stress, this could result in lowering further the specific deposit and the normalized pressure drop in the fixed bed section. This was confirmed by the measured profiles of Figures 5a, b. The similarity in fitted diameters for both runs stipulates according to Eq. 14 that the critical shear stress would be indifferent to an increase in U_{Lsf}. However, the wall shear stress τ_w intervening in the detachment rate Eq. 13 would increase linearly with U_{Lsf}.[26] This means that for U_{Lsf} = 0.064 m/s, had α^h_{det} taken the value 1.5×10^{-8} s/m would have meant less reentrainment of solids resulting in higher normalized pressure drop and specific deposits than actually measured. This indicates that a model for the hydrodynamic detachment rate given by Eq. 13 seems not totally adequate with a velocity-independent α^h_{det} parameter. Velocity-dependent α^h_{det} parameter on the contrary indicates that "softer," hence easily detachable, deposits form in the fixed bed at higher semifluidization velocity. Recalling that R = 2 and H_F was virtually constant (Figure 5), an increase of U_{Lsf}, namely, increasing the fluidized section porosity, seemed to play a role in softening the deposited particles in the fixed bed section.

Figure 6 expresses the evolution as a function of bed specific deposit of the overall capture efficiency, E (Eq. 3), and the global filter coefficient, $\langle\lambda\rangle$ (Eq. 6). Both are decreasing functions of the semifluidization velocity in agreement with literature studies.[9,10,21] Both exhibited a plateau stretching over a wide specific deposit range before E and $\langle\lambda\rangle$ turned into decreasing functions of the specific deposits. The higher the U_{Lsf} the briefer the plateau: up to *ca.* 35, 30, and 10 kg/m^3 for, respectively, 0.028, 0.042, and 0.064 m/s. The filter coefficient curves did not reach steady-state filter coefficient values with increasing filtration time or specific deposit. However, the E vs. σ dependence was similar to that observed for carbon black/kerosene suspensions[21] though our E and $\langle\lambda\rangle$ values were typically an order of magnitude lower because of ten times higher velocities in the present study. The theoretical initial filter coefficients, $\lambda_o(\sigma = 0)$, computed

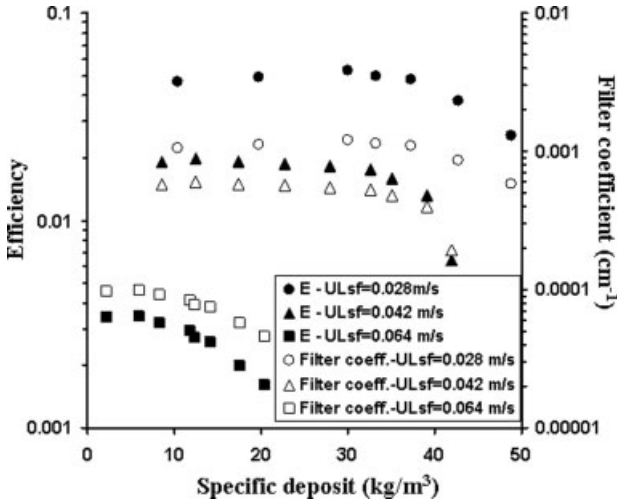

Figure 6. Effect of suspension semifluidization superficial velocity on overall capture efficiency and global filter coefficient vs. specific deposit (U_{Lsf} = 0.028 m/s; H_F = 0.3 m), (U_{Lsf} = 0.042 m/s, H_F = 0.33 m), (U_{Lsf} = 0.064 m/s, H_F = 0.33 m), R = 2.

using the correlation of Rajagopalan and Tien[29] with d_f = 8 μm gave 1.44×10^{-3}, 1.14×10^{-3}, and 9.38×10^{-4} cm^{-1} for U_{Lsf} = 0.028, 0.042, and 0.064 m/s, respectively. The limiting filter coefficients extrapolated towards $\sigma \to 0$ from the global filter coefficients in Figure 6 were correspondingly, 0.94×10^{-3}, 0.53×10^{-3}, and 10^{-4} cm^{-1}. The initial filter coefficient values λ_o were systematically higher with respect to those extrapolated from the bed-length averaged $\langle\lambda\rangle$ values. However, they remained pair-wise reasonably close except for the largest semifluidization velocity. Since $\langle\lambda\rangle$ is a crude parameter lumping deposition and reentrainment alike it allows only gross descriptions complementary to the analysis via the depth filtration model used above. Using the Rajagopalan and Tien[29] and Tien et al.[30] filter coefficients in the depth filtration model revealed softening of the deposit with increasing U_{Lsf} as indicated by the larger values of $\alpha^h{}_{det}$. Such dependence of deposit structure was also indirectly revealed by the lower extrapolated value of $\langle\lambda\rangle$ for U_{Lsf} = 0.064 m/s.

Effect of split ratio on fines deposition

A series of filtration runs was conducted to assess the influence of split ratio on the evolution of pressure drop and specific deposit in semifluidization. To prevent deposition in the lowermost fluidization section, a semifluidization velocity of 0.042 m/s was chosen for split ratios R = 1 (H_F = 0.25 m), R = 2 (H_F = 0.34 m), R = 3 (H_F = 0.34 m), and $R = \infty$ (H_F = 0.42 m), that is, solitary fixed bed. Note that only R = 2 and R = 3 runs could be compared in terms of filtration as they have the same fixed bed height, H_F.

An increase in R led to an increase in the time required to magnify by a commensurate factor the normalized pressure gradient (Figure 7a). This is also reflected by the lesser solids retention in the fixed beds with increasing R ratios (Figure 7b). Similarly, the overall capture efficiency and the global

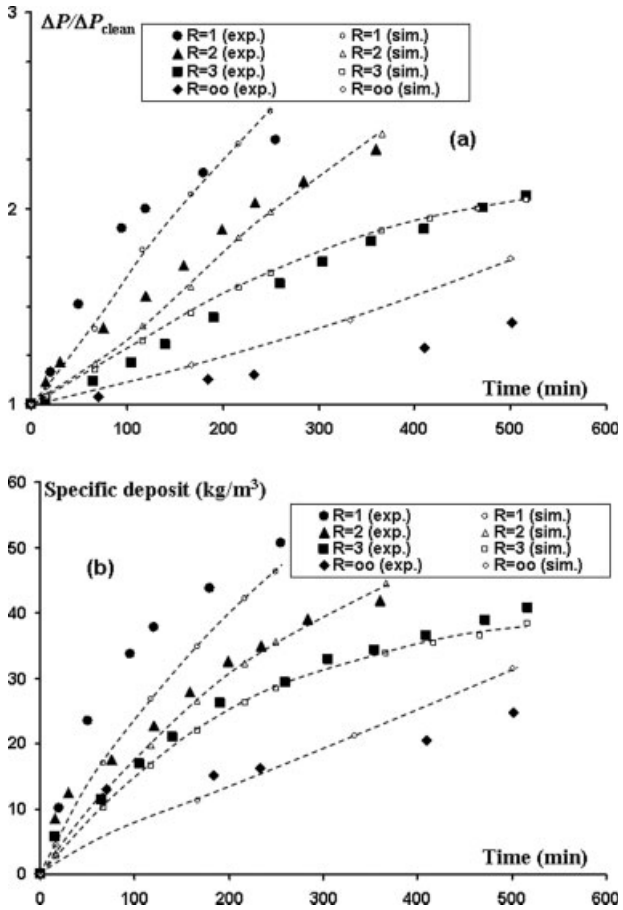

Figure 7. Effect of split ratio on (a) normalized pressure drop vs. time, (b) specific deposit vs. time (R = 1; H_F = 0.25 m), (R = 2; H_F = 0.34 m), (R = 3; H_F = 0.34 m), (R = ∞; H_F = 0.42 m), U_{Lsf} = 0.042 m/s.

Dotted lines/empty symbols shows simulations by depth filtration model Eqs. 7–14.

filter coefficient decreased with increasing split ratios (Figure 8). Interestingly, the filter coefficient for the solitary fixed bed ($R = \infty$) reached a steady-state value, that is, σ- and time-invariant values, coherent with the observations made in earlier works with similar organic liquids.[9,21]

The heights of the fixed bed layers were shorter by 60–80% with respect to the solitary fixed bed ($R = \infty$) and exhibited higher normalized pressure drops and specific deposits. Such increases cannot be ascribed only to the fact that shorter beds cause lesser disparities than taller beds. The capture in the upper fixed bed was not indifferent to the presence of a fluidized section, see the runs at $R = 2$ and 3 with constant H_F. At constant ε_{So}, shallower fluidized sections helped delaying deposition in the adjacent fixed bed (Figure 7b). This also improved the system's resilience to capture as indicated from decreased filter coefficient and capture efficiency (Figure 8). Two opposite factors could likely be at the origin of such R-dependences of capture dynamics. A fluidization-controlled aggregation turning fines into larger aggregates easily trappable in the adjacent fixed bed which is not desirable. A fluidization-induced softening of the deposits to build up in the contiguous fixed bed prompting larger hydrodynamic release rate coefficients as evidenced with regard to the effect of U_{Lsf}. Analysis of the simulation data by the depth filtration model, Eqs. 7–14, leaned in favor of both scenarios as will be discussed later.

The dotted lines connecting the empty symbols in Figures 7a, b were the simulated normalized pressure gradients, $\Delta P/\Delta P_{clean}$, and their corresponding specific deposits, σ, for different split ratios. For $R = \infty$, the fitted diameter d_f was 1 μm which led to acceptable fits for the dimensionless pressure drop and corresponding specific deposit. The largest aggregate sizes were observed for the run at $R = 1$, where $d_f = 20$ μm and $\alpha^h_{det} = 1.5 \times 10^{-8}$ s/m. Whereas, the runs at $R = 2$ and 3, yielded, respectively, $d_f = 8$ μm and $\alpha^h_{det} = 1.5\times10^{-8}$ s/m, and $d_f = 8$ μm and $\alpha^h_{det} = 7 \times 10^{-8}$ s/m. Therefore, the much larger hydrodynamic release rate for $R = 3$, though d_f remained invariant as for $R = 2$, tends to confirm that shallower (but iso-ε_{So}) fluidized beds prompted the formation of softer deposits. Thus, lesser net solids trapping occurred in the adjacent fixed bed. At first sight and despite precautions to delineate workable semifluidization conditions, the increasing aggregate sizes would be a negative effect induced by fluidization. However, as will be seen next, this would not represent an obstacle owing to the flexibility of semifluidization units (Figure 1) to enable self-cleaning.

Effect of cyclic operation parameters on alternating semifluidization mode

Three successive cycles were run for each of the three cyclic operation parameters summarized in Table 1, namely, the washing time, the suspension washing velocity, U_L, and the washing gas velocity, U_G. All the experiments were carried out at $R = 1$ during filtration and at $R = 0$ for unconstrained fluidization during the washing stage. The system's

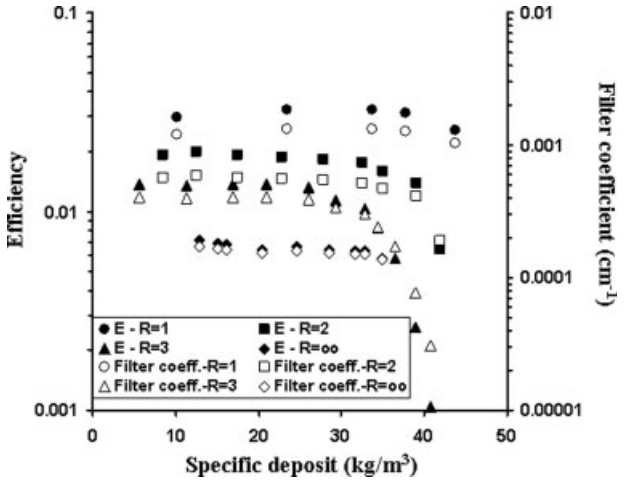

Figure 8. Effect of split ratio on overall capture efficiency and global filter coefficient vs. specific deposit (R = 1; H_F = 0.25 m), (R = 2; H_F = 0.34 m), (R = 3; H_F = 0.34 m), (R = ∞; H_F = 0.42 m), U_{Lsf} = 0.042 m/s.

Table 1. Effect of Cyclic Operation Parameters in Alternating Semifluidization Mode ($R = 1$)

	1st Cycle Filtration Time,[1] Ft_I (min)	Ft_{II}/Ft_I (%)	Ft_{III}/Ft_I (%)
Washing time[2] (min) (Figure 9)			
2	870	35.1	27.7
10	893	28.9	24.8
20	885	30.9	19.9
Washing velocity,[3] U_L (m/s) (Figure 10)			
0.015	885	23.6	12.7
0.027	885	26.9	19.9
0.037	885	30.9	22.9
Washing gas velocity,[4] U_G (m/s) (Figure 11)			
0.006	885	33.9	32.4
0.032	885	37.6	34.9
0.098	885	37.5	35.5

Suspension washing velocity: $U_{Lmf} < U_L < U_{Lmsf}$; Ft_i = ith cycle filtration time.
[1]Filtration time elapsed for the pressure drop to double.
[2]U_{Lsf} = 0.055 m/s, suspension washing velocity, U_L = 0.027 m/s*.
[3]U_{Lsf} = 0.055 m/s, Washing time = 20 min.
[4]U_{Lsf} = 0.055 m/s, U_L = 0.027 m/s, Washing time = 20 min.

performance was assessed in terms of the fractions of filtration times Ft_{II}/Ft_I and Ft_{III}/Ft_I of second and third cycles with respect to first cycle, respectively, after which the pressure drop in the fixed bed section doubled with respect to ΔP_{clean}.

Figures 9a, b illustrate the evolution of normalized pressure drop and specific deposit as a function of time on stream for three different values of the washing time, Wt: 2, 10, and 20 min. The time evolution in 1st cycle of $\Delta P/\Delta P_{clean}$ and σ was indicative of a very good experimental reproducibility, see Table 1. The semifluidization velocity was 0.055 m/s to prevent unwanted capture within the fluidization section. Specific deposits as high as 100 kg/m^3 could be attained (Figure 9b). For each value of Wt (2, 10, or 20 min), two more cycles (Ft_{II} and Ft_{III}) were performed. After detachment of deposits and cleaning of the bed during the washing stage at U_L (wash) = 0.027 m/s, the semifluidized bed state was resumed by setting up again U_{Lsf} (see Figure 9a). This was accompanied by a sudden turbidity burst in the tank which enabled retrieving, for the subsequent cycles, virtually the solids concentration as in the starting suspension (results not shown). This provided postfacto confirmation of the brevity of washing times in unconstrained fluidization indicating negligible capture during the washing stage. Regardless of washing time, the filtration time required for doubling the initial pressure drop decreased with the number of cycles (Table 1). Moreover, for a given higher cycle, an increase in washing time resulted in faster plugging of the fixed bed section (Table 1). For better results, it would advisable for the inter-cycle washing time to be reduced. Destruction of fixed bed deposits and their liberation during the washing period underlined the larger sizes of the released aggregates. This entrained shortening of the higher cycles.

Figure 10 illustrates the evolution of normalized pressure drop as a function of time on stream for different suspension washing velocities, U_L (wash). Similarly, Figure 11 highlights the influence of washing gas superficial velocity in full three-phase fluidization conditions with U_L = 0.027 m/s. The intermittence between filtration stages (Ft_I to Ft_{III}) and washing stages (during the periods Wt) is shown in Figures 10 and 11. The semifluidization velocity was 0.055 m/s and a constant washing time of 20 min was used. Similar shorten-

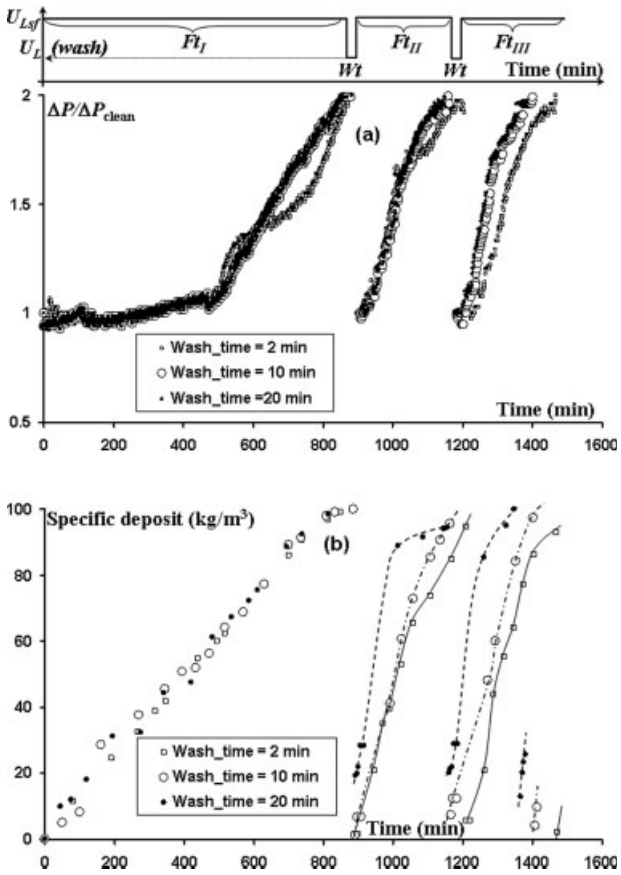

Figure 9. Effect of washing time on: (a) normalized pressure drop in fixed bed section, (b) and specific deposit vs. time-on-stream.

U_{Lsf} = 0.055 m/s, U_L = 0.027 m/s, R = 1. Lines show trend.

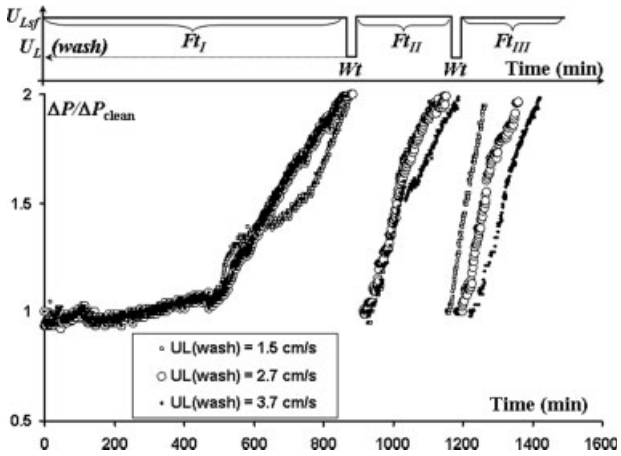

Figure 10. Effect of suspension washing velocity on normalized pressure drop in fixed bed section vs. time-on-stream. U_{Lsf} = 0.055 m/s, washing time = 20 min, R = 1.

Lines show trend.

ing of subsequent cycle durations was noticed for the same reasons explained above. For a given washing suspension velocity, the filtration time required for doubling the initial pressure drop decreased with the number of cycles, Table 1. However, the most severe loss in filtration time occurred with lowering the washing suspension velocity. For a given higher cycle, a decrease in washing suspension velocity resulted in faster trapping by the fixed beds (Figure 10). Introduction of gas during the washing stage brought significant improvements in preserving the filtration time as seen in Table 1. In this case, the filtration time remained relatively constant around 35% regardless of the cycle by increasing U_G from 0.006 to 0.098 m/s. These U_G seemed effective in reducing the sizes of the aggregates below the sizes in the gas-free flow washing stages (Figures 9 and 10).

Carrying out single-pass alternating semifluidization experiments for ca. 3000 min would have required ca. 25 m^3 of fresh suspension. This was obviously out of reach for our lab-scale facility. For lack of implementing true suspension single-pass flows, we resorted to a strategy which consisted in replacing the recycled suspensions on the verge of each new cycle by a fresh one. This is shown for three cases in Figure 12: surfactant-free suspension at $R = 1$, surfactant-stabilized suspension at $R = 1$ and 1/6. The semifluidization and washing suspension velocities were $U_{Lsf} = 0.055$ m/s and $U_L = 0.027$ m/s, respectively. As can be seen in Figure 12, the fractions of filtration times Ft_{II}/Ft_I and Ft_{III}/Ft_I of second and third cycles with respect to first cycle remained close to 100%. This confirms the potential of a self-cleaning alternating semifluidized bed to periodically get rid of deposits without requiring unit shutdown. Figure 12 reveals relatively fast deposition and doubling of pressure drop from a surfactant-free suspension compared to the surfactant-stabilized suspension. The filtration time corresponded typically to 20 recirculation times from tank to column for surfactant-free suspensions and 100 recirculation times for surfactant-

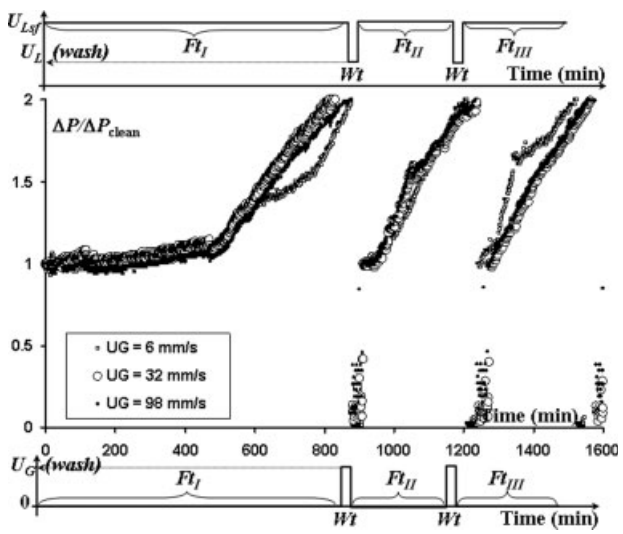

Figure 11. Effect of washing gas velocity on normalized pressure drop in fixed bed section vs. time-on-stream.

$U_{Lsf} = 0.055$ m/s, $U_L = 0.027$ m/s washing time = 20 min, $R = 1$. Lines show trend.

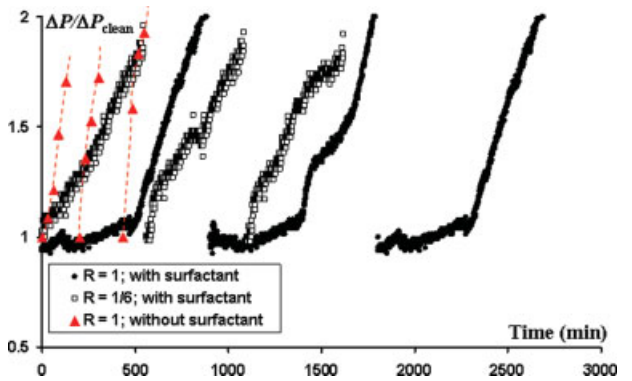

Figure 12. Proof of concept of self-cleaning alternating semifluidization with replacement of fresh (surfactant-stabilized and surfactant-free) suspensions at each new cycle: normalized pressure drop in fixed bed section vs. time-on-stream.

$U_{Lsf} = 0.055$ m/s, $U_L = 0.027$ m/s, ($H_F = 5$ cm, $R = 1/6$), ($H_F = 10$ cm, $R = 1$). Lines show trend.
[Color figure can be viewed in the online issue, which is available at www.interscience.wiley.com.]

stabilized ones. The use of surfactant appeared to efficiently retard the growth of aggregate diameter primed in the fluidization section for some two-thirds of the recycles (ca. 65%) with the characteristic induction phase shown in Figure 12. It was followed by a sudden surge in pressure drop as without surfactant (Figure 12). Although it was not specifically investigated, this phenomenon was speculated to result from progressive depletion of surfactant around suspended particles. This would be caused after the release mechanism would have liberated fines attached to the *porous* catalyst collectors which had already adsorbed some of the surfactant. It is interesting to note that the induction period was totally eliminated from the pressure drop dynamic curves when the split ratio was 1/6. This result confirms the observation above regarding the necessity of using *shallow* fluidized sections to move away plugging of the fixed bed section. Because of its six-fold larger height with respect to fixed bed, over-production of aggregates in the fluidization section became quickly overwhelming for the fixed bed section.

Conclusion

This study was about the feasibility of an alternating semifluidized bed to allay the problem of plugging with fines. This was made possible by switching the suspension velocity between a velocity $> U_{Lmsf}$ during capture, and a lower velocity $> U_{Lmf}$ whereby full fluidization was restored to allow removal of deposits. The following conclusions can be drawn regarding filtration in semifluidization:

- A threshold solids holdup was identified below which capture of fines in the fluidization section was not allowed. This threshold corresponded to a solids holdup of 15–20% in unconstrained fluidization and 32% in constrained fluidization.
- Analysis with a depth filtration model accounting for solids detachment revealed that the fluidization section was

not neutral. It favored growth of the aggregate size entering the fixed bed section.

- The split ratio was found also to affect the capture dynamics. Higher split ratios tended to decrease the normalized pressure gradient and specific deposits. For a constant fixed bed height, the shallowest fluidization sections helped delaying deposition in the adjacent fixed bed.
- In cyclic operation, reversibility of the alternating semifluidized bed was best recovered by injection of gas during the washing cycles. The filtration times in the subsequent cycles were decreasing functions of washing time and increasing functions of the washing superficial velocity of suspensions.
- The use of fresh suspensions in single-pass mode appeared to behave very well under cyclic operation even without injecting gas during the washing cycle. This remained true regardless of whether surfactant-free or surfactant-stabilized suspensions were tested.
- Only two studies from Professor's L.S. Fan group have been found regarding the hydrodynamics of filtration-free three-phase semifluidization.[15,33] The next step will be to study the concept of alternating semifluidization under three-phase conditions to mimic actual hydrotreating cases.

Acknowledgments

Financial support from the Natural Sciences and Engineering Research Council of Canada Strategic Grant Program is gratefully acknowledged.

Notation

C = suspension concentration, kg/m^3
D = column diameter, m
d_f = fine diameter, m
d_P^0 = clean collector diameter, m
D_L = axial dispersion coefficient in suspension phase, m^2/s
E = overall capture efficiency
F_{LS} = liquid-solid drag force, N/m^3
H_F = fixed bed height section, m
h_f = fluidized bed height section, m
h_o = fixed bed height at rest, m
H_o = semifluidized bed height, m
L = bed length, m
N = filtration rate, reactor volume basis, s^{-1}
P = pressure, Pa
Q = suspension volumetric flow rate, m^3/s
r = detachment rate, s^{-1}
R = split ratio, H_F/h_f
v_{Lsf} = interstitial semifluidization velocity, m/s
t = time, s
U_{Lmf} = minimum fluidization superficial velocity, m/s
U_{Lmsf} = minimum semifluidization superficial velocity, m/s
U_{Lsf} = semifluidization superficial velocity, m/s
U_∞ = terminal velocity, m/s
V_R = reactor volume, m^3
V_T = volume of suspension in tank, m^3
z = axial coordinate in bed, m

Greek letters

α_{det}^c = colloidal 1st-order release rate coefficient, s^{-1}
α_{det}^d = hydrodynamic release rate coefficient, s/m
ΔP_{clear} = pressure drop in clean bed, Pa
ΔP = pressure drop during bed plugging, Pa
ΔP_{max} = maximum pressure drop during bed plugging before resuming washing stage, Pa
ε = bed porosity
ε_{So} = initial solids holdup in fluidized section
ε_f = porosity of fluidized section
γ = fraction of collector surface area available for adhesion
$\langle\lambda\rangle$ = bed averaged filter coefficient, m^{-1}
λ = local filter coefficient, m^{-1}
μ = dynamic viscosity, Pa s
ρ = density, kg/m^3
σ = specific deposit, mass of fines per unit bed volume, kg/m^3 or (reactor volume basis) m^3/m^3
τ = shear stress on collector plan, N/m^2

Subscripts

c = collector
cr = critical
d = deposit
det = detachment
f = fine
G = gas
In = inlet
L = liquid
mf = minimal fluidization
msf = minimal semifluidization
Out = outlet
s = solid
w = wall

Superscripts

o = clean bed state, at rest
c = colloidal
h = hydrodynamic

Literature Cited

1. Flint L. Bitumen and very heavy crude upgrading technology. A review of long term opportunities. *Petroleum Technology Alliance Canada*, January 2005. Available at www.ptac.org/. Last accessed, May 29, 2008.
2. Strausz OP, Lown, EM. *The chemistry of Alberta oil sands, bitumens and heavy oils*. Alberta Energy Research Institute. Calgary, Alberta, Canada, 2003.
3. Bauquis PR. A reappraisal of energy supply and demand in 2050. *The Institute of Energy Economics*, Japan, July 2002. Available at http://eneken.ieej.or.jp/en/outlook/. Last accessed, May 29, 2008.
4. Cupcic F. Extra heavy oil and bitumen: the challenges of enhanced recovery. ASPO Meeting, France, May 2003.
5. Lepage JF, Chatila SG, Davidson M. *Raffinage et conversion des produits lourds du pétrole*. Paris: Édition Technip, 1990.
6. Sundaramurthy V, Dalai AK, Adjaye J. HDN and HDS of different gas oils derived from Athabasca bitumen over phosphorus-doped NiMo/γ-Al_2O_3 carbides. *Appl Catal B: Environmental*. 2006;68:38–48.
7. Koyama H, Nagai E, Torii H, Kumagaio H. Simple changes reduce catalyst deactivation, pressure-drop buildup. *Oil Gas J*. 1995;93:68–71.
8. Gray MR, Srinivasan N, Masliyah JH. Pressure buildup in gas-liquid flow through packed beds due to deposition of fine particles. *Can J Chem Eng*. 2002;80:346–354.
9. Edouard D, Iliuta I, Larachi F. Role of gas phase in the deposition dynamics of particles in trickle-bed reactors. *Chem Eng Sci*. 2006; 61:3875–3884.
10. Hamidipour M, Larachi F, Ring Z. Hydrodynamic observations of trickle beds under filtration conditions. *Ind Eng Chem Res*. 2007; 46:8336–8342.
11. Hamidipour M, Larachi F, Ring Z. Three-phase monoliths versus trickle beds: comparative studies of gas-liquid filtration behavior. *Chem Eng Sci*. 2007;62:5538–5542.
12. Fan LT, Wen CY. Method of wastewater treatment in fluidized bed biological reactors. US Patent 4,253,947, March 1981.
13. Fan LS. *Gas-Liquid-Solid Fluidization Engineering*. Stoneham, MA: Butterworth Publishers, 1989.
14. Fan LT, Yang YC, Wen CY. Semifluidization: mass transfer in semifluidized beds. *AIChE J*. 1959;5:407–409.

15. Chern SH, Fan LS, Muroyama K. Hydrodynamics of cocurrent gas-liquid-solid semifluidization with a liquid as the continuous phase. *AIChE J*. 1984;30:288–294.
16. Hristov J. Magnetic field assisted fluidization - A unified approach - Part 2. Solids batch gas-fluidized beds: versions and rheology. *Rev Chem Eng*. 2003;19:1–132.
17. Wen CY, Fan LT. Method of filtration using convertible (semifluidized) beds. US Patent 4,157,959, June 1979.
18. Fan LT, Hsu EH. Method of filtration using semifluidized beds. US Patent 4,438,000, March 1984.
19. Larachi F, Cassanello M, Chaouki J, Guy C. Flow structure of the solids in a three-dimensional gas-liquid-solid fluidized bed. *AIChE J*. 1996;42:2439–2452.
20. Tanabe K, Gray MR. Role of fines solids in the coking of vacuum residues. *Energy Fuels*. 1997;11:1040–1043.
21. Narayan R, Coury JR, Masliyah JH, Gray MR. Particle capture and plugging in packed-bed reactors. *Ind Eng Chem Res*. 1997;36:4620–4627.
22. Tien C. *Granular Filtration Of Aerosols And Hydrosols*. Boston, MA: Butterworth-Heinemann Series in Chemical Engineering, 1989.
23. Ryan JN, Gschwend PM. Effects of ionic strength and flow rate on colloid release: relating kinetics to intersurface potential energy. *J Colloid Interface Sci*. 1994;164:21–34.
24. Khilar KC, Fogler HS. *Migration of Fines in Porous Media*. Dordrecht, The Netherlands: Kluwer Academic Publishers, 1998.
25. Dankworth DC, Kevrekidis IG, Sundaresan S. Dynamics of pulsing in trickle beds. *AIChE J*. 1990;36:605–621.
26. Iliuta I, Larachi F. Stretching operational life of trickle-bed filters by liquid-induced pulse flow. *AIChE J*. 2005;51:2034–2047.
27. Iliuta I, Larachi F. Fines deposition dynamics in packed-bed bubble reactors. *Ind Eng Chem Res*. 2003;42:2441–2449.
28. Iwasaki T. Some notes on sand filtration. *J Am Water Works Ass*. 1937;29:1591–1602.
29. Rajagopalan R, Tien C. Trajectory analysis of deep-bed filtration with the sphere-in-cell porous media model. *AIChE J*. 1976;22:523–533.
30. Tien C, Turian RM, Pendse H. Simulation of the dynamic behavior of deep bed filters. *AIChE J*. 1979;25:385–404.
31. Arulanandan K, Longanathan P, Krone KB. Pore and eroding fluid influences on surface erosion of soil. *J Geotech Eng Div ASCE*. 1975;101:51–65.
32. Choo CU, Tien C. Analysis of the transient behavior of deep-bed filtration. *J Colloids Interface Sci*. 1995;169:13–33.
33. Chern SH, Fan LS, Muroyama K. Hydrodynamics of cocurrent gas-liquid-solid semifluidization with a liquid as the continuous phase. *Chem Eng Sci*. 1983;38:1167–1174.

Manuscript received Aug. 20, 2007, revision received Jan 30, 2008 and final revision received May 2, 2008.